Available online at www.sciencedirect.com

SciVerse ScienceDirect

Energy Procedia 37 (2013) 4191 – 4198

Energy Procedia

GHGT-11

Microseismic monitoring and interpretation of injection data from the In Salah CO_2 storage site (Krechba), Algeria

Volker Oye[a)], Eyvind Aker[b)]*, Thomas M. Daley[c)], Daniela Kühn[a)], Bahman Bohloli[b)], Valeri Korneev[c)]

[a] NORSAR, Gunnar Randers vei 15, 2007 Kjeller, Norway
b Norwegian Geotechnical Institute, Sognsveien 72, 0855 Oslo, Norway
c Lawrence Berkeley National Laboratory, CA, USA

Abstract

Microseismic data analysis together with interpretation of injection data at the In Salah CO_2 storage site provides a valuable tool for improved understanding of the subsurface injection and storage processes. More than 1500 microseismic events have been detected semi-automatically between August 2009 and May 2012 and the occurrence of the events correlates clearly with increased injection rates and well-head pressures. Most likely the fracture pressure has been exceeded temporarily, resulting in a sudden increase of microseismicity. Waveform cross-correlation of the events demonstrates that most events occur in three distinct clusters. Clusters with shorter S-P wave differential travel times clearly correlate with the CO_2 injection at KB502, whereas events with larger S-P wave times do not. An uncertainty analysis and a network design study conclude that a more extensive microseismic network would be needed to resolve locations and potential correlations with injection data.

Selection and/or peer-review under responsibility of GHGT

Keywords: CO_2 storage; injection; monitoring; microearthquakes; seismicity; fracturing; instrumentation

Introduction

At the industrial-scale CO_2 capture and storage project at In Salah (Krechba), Algeria, microseismic monitoring has been tested as a potential technique to detect microseismic activity associated with injecting CO_2 into the subsurface. At Krechba, CO_2 injection started in 2004 and three wells (KB501, 502 and 503) are used to inject into the same ~20 m thick saline Carboniferous reservoir along horizontal well sections that are up to 1.8 km long. The porosity of the reservoir sandstone is between 10 and 17% and the permeability is about 10 mD [1]. The reservoir is covered by 950 m thick Carboniferous mudstones, and tight siltstone and sandstones which act as seals for the storage unit. Another 900 m thick sequence of Cretaceous sandstone and mudstones covers the sealing formations. Ground surface deformation from InSAR measurements shows that the CO_2 injection is accompanied by surface uplift and various

1876-6102
Selection and/or peer-review under responsibility of GHGT
doi:10.1016/j.egypro.2013.06.321

numerical simulators coupling CO_2 flow and rock deformation have been developed to confirm the observations (e.g. [2], [3], [4], [5]). Rutqvist et al. [4], inferred that there is a relatively low potential for injection-induced microseismicity at In Salah, however, they pointed out that only small variations in the assumed maximum horizontal effective stress could change their conclusions. Gemmer et al. [5] showed in a geomechanical study that a fully elastic model could only account for about half the amount of observed surface uplift and that fractures were required to explain the double-lobe uplift feature at well KB502, as proposed by Vasco et al. [2].

Microseismic monitoring is routinely applied in the mining industry as well as in hydraulic fracturing operations in the oil and gas industry, e.g. in shale-gas extraction. It is also successfully employed during the creation of enhanced geothermal reservoirs. The microseismic events can be located and classified using well-established methods developed in seismology. Such interpretation of microseismic data, i.e. the locations of events and their source parameters (like magnitude, frequency content, seismic/elastic energy) in combination with injection rate and pressure data can provide valuable information about processes related to injection and fracturing within the reservoir.

In this paper we present results from the KB601 microseismic pilot well [6] and related CO_2 injectivity data. We show that substantial microseismic activity was recorded in the vicinity of the KB502 well during 2010 and 2011. The analysis of pressure versus injection rate shows that pressures in all three wells have most probably exceeded the fracture pressure of the injection horizon for limited periods of time. The observed microseismic activity from 2010 appears to correlate well with CO_2 pressure and injection rates at the KB502 well-head. However, a major extension of the microseismic network would be needed to significantly improve the accuracy of source locations and enable advanced source parameter estimation.

Instrumentation and data analysis

A one dimensional array consisting of 48 three-component downhole geophones was deployed in a single vertical well (KB601), ranging from about 30 to 500 m depth with 10 m spacing. Geophones from six levels have been connected to three digitizers from REF-TEK, recording continuous waveform data at 500 Hz sampling frequency since August 2009. Orientation of the sensors has been achieved through repeated hammer strike tests around the borehole. During a field visit in June 2011, it was established that only two (at approx. 80 and 160 m depth) of the six connected geophones provided reliable data and only the geophone deployed at 80 m depth could be oriented successfully. The data were contaminated by electronic spikes and the seismic traces were not aligned in time due to partly malfunctioning GPS units. After signal processing to remove undesirable electronic and rural noise, the continuous data have been processed automatically to identify microseismic events. Despite the poor data quality, more than 1500 events have been identified throughout 2010.

In June 2011, the geophone cables were reworked at the well-head and six fully functional levels of 3-component geophones were established. In November 2011, the three REF-TEK digitizers were replaced by one digitizer from Kinemetrics recording continuously eight 3-component geophones at a common GPS time. The electronic noise was significantly reduced, probably because the Kinemetric digitizer was put close to the well-head enabling shorter cables for transferring the analogue signals from the geophones to the digitizer. Repeated hammer strikes around the borehole were used to calibrate the new eight levels of geophones, ranging from 80 to about 250 m depth. An example of a microseismic event recorded with the Kinemetrics setup is shown in Figure 1.

Results of microseismic monitoring analysis

The observed microseismic activity from 2010 correlates with high CO_2 pressure and high injection rates at the well-head (Figure 2). During two periods in June and July 2010, the fracture pressure was exceeded (indicated by the red horizontal line) and the observed seismicity increased immediately. Peak activity rates of 20-40 events per day were observed based on automatic classification. CO_2 injection was temporarily suspended in June 2011, causing the microseismic activity to decrease significantly. However, about 10-20 detectable microseismic events per month were recorded from June to October 2011. Unfortunately, the one-dimensional geometry of the array with limited aperture from 80 to 250 m depth (which before June 2011 was limited to only two geophones at 80 and 160 m depth) does not allow for accurate microseismic event location. The events were detected using an automated P- and S-wave phase onset picking and P- and S-wave polarization analysis similar to the methods described in Oye and Roth [7]. In order to obtain a crude estimate of the direction and distance of the most likely event locations, we plotted S-P arrival time differences as a proxy for distance to the observation well and the polarization angle of the P-wave onset. Events that are further away (S-P ~ 900 ms) do not correlate with injection rates at KB502, whereas events with shorter distance to the observation well appear to strongly correlate with injection rates at KB502. Figure 4 shows the azimuthal distribution of S-P wave arrival time differences. The majority of the events occur along an azimuth aligned with the direction of the largest horizontal stress.

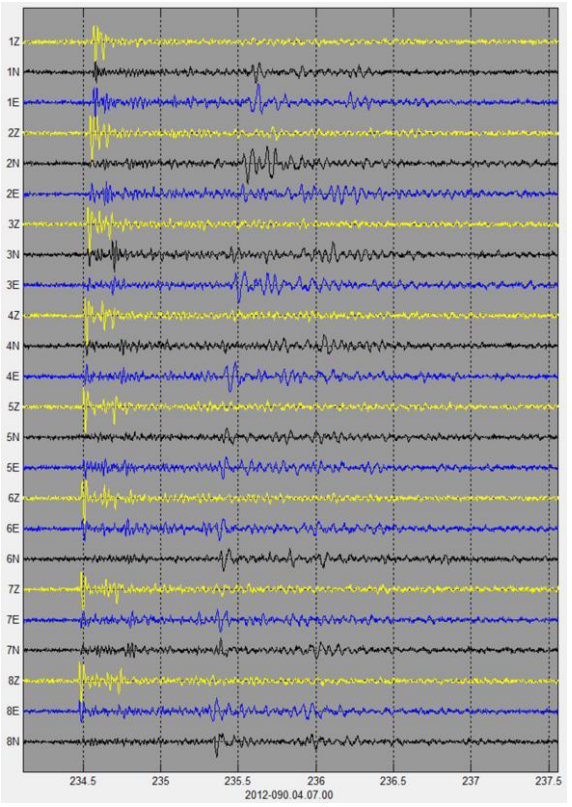

Fig. 1. Example of a microseismic event recorded within well KB601 on 31 March 2012, clearly seen on all channels (Z: vertical component, yellow; N: North component, black; E: East component, blue). Geophone 8 is deployed deepest (approx. 244 m depth) in the well and geophone 1 is shallowest (approx. 52 m depth). The P-wave (at ~234.5 s) and S-wave arrivals (at ~235.5 s) are clearly visible on all channels. In addition, surface reflected P-waves, P-to-S converted waves as well as S reflected waves are visible.

To estimate uncertainty in microseismic event locations, we compute the wave fields at each sensor in a layered velocity model using an elastic 2-D finite-difference method. To save computation time we take advantage of the reciprocity theorem, i.e. we place theoretical sources in the geophone positions and receivers in every node of the velocity model, while travel times and incidence angles remain unchanged. Therefore, just two runs per level allow us to determine the space-dependent fields t_{Pi}, t_{Si} and θ_i, which are P- and S-wave travel times and P-wave incident angle, respectively; index i (i=1,2,3,4) denotes the receiver level. By normalizing S-P time and incident angle to give a percentage misfit, we can calculate a combined misfit using both angle and time. This gives the estimated error (uncertainty) at each point in the model for a given microseismic event location, as shown in Figure 5. For an event with a measurement error of 10-20% in travel time and polarization, we have up to 1 km uncertainty in location, assuming the velocity model is correct.

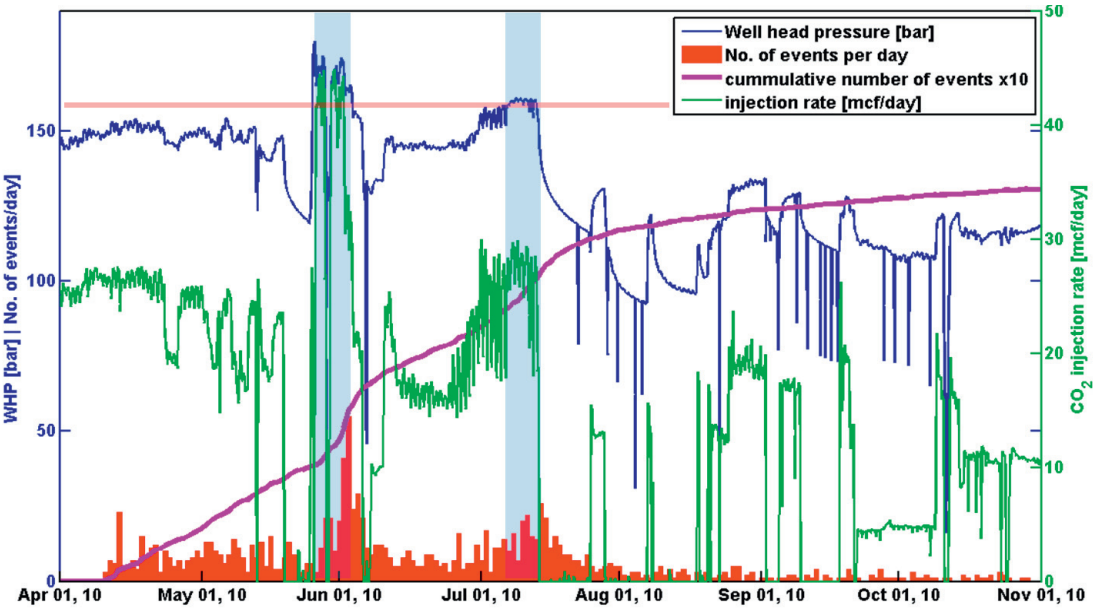

Fig. 2. Temporal evolution of CO_2 injection rate, well-head pressure and microseismic events. A clear increase in microseismic activity of more than about 20 detected events per day coincides with high injection rates and high well-head pressures. The horizontal red line indicates fracture pressure.

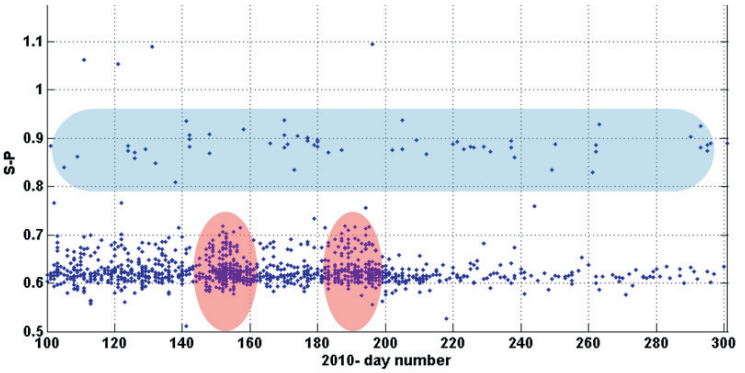

Fig. 3. Temporal evolution of S-P arrival times (day 100 corresponds to 10th of April and day 300 to 27th of October 2010). Events with S-P arrival times of 600 – 700 ms are more frequent during times of high injection rates and quickly decrease after injection decreased. Events with larger S-P arrival time differences of ~900 ms do not show any correlation to injection rates at KB502.

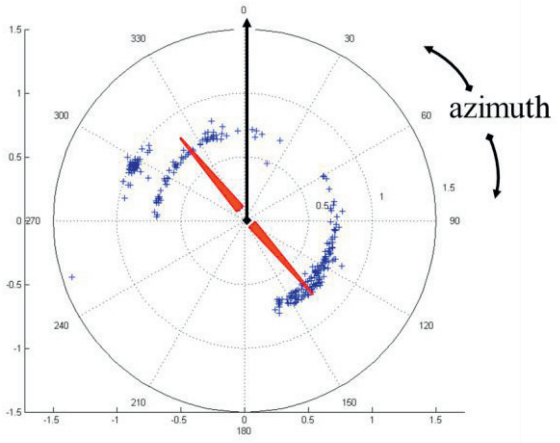

Fig. 4. Estimated S-P arrival time differences (blue dots) plotted in a rose-diagram. The distance to the center represents the S-P times and the azimuth describes the direction where the events originate as seen from the observation well. The regional stress field is indicated by red arrows, pointing in direction of the largest horizontal stress, σ_{Hmax}.

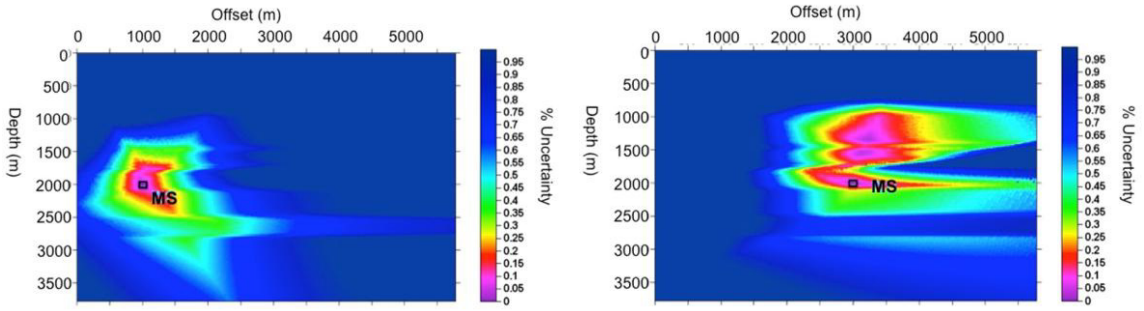

Fig. 5. Calculated uncertainty in event location for an event at 2 km depth and an offset from sensor well of 1 km (left) and 3 km (right). Uncertainty was calculated separately for S-P time and incident angle, and then added for combined uncertainty (misfit error). The actual location of the numerically modeled event is shown as a dot labeled MS.

Further analysis of the microseismic waveform data using cross-correlation techniques indicates that most events occur within distinct spatial clusters. High waveform cross-correlation values between two events generally indicate that the events have a similar source mechanism and travel paths, i.e. they originated at similar locations. From Figure 6, we can extract three distinct clusters with high cross-correlation values (red colors) and about 200 events that do not correlate with the main clusters. The two largest clusters belong to the events with 600-700 ms S-P wave travel time difference, the third, smaller cluster is the one with ~900 ms S-P travel time difference.

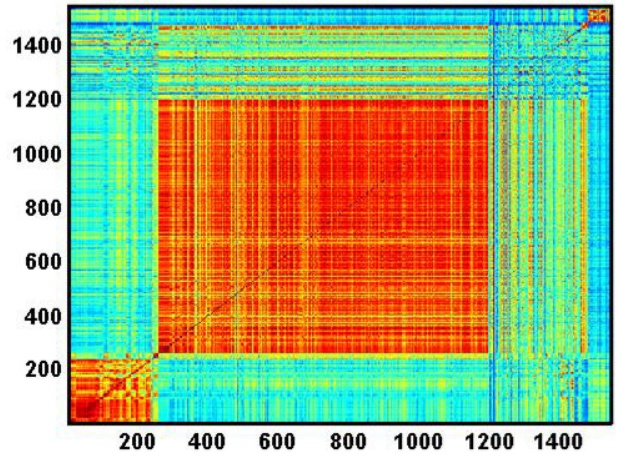

Fig. 6. Cross-correlation matrix computed from vertical component waveform data of all detected events in 2010. High values (close to 1) are colored red, small values (close to 0) are blue. Three distinct clusters can be identified (events 1-240; 241-1200; 1400-1500). High cross-correlation values represent high similarity between the waveforms, which indicates that the events have occurred close to each other, with a similar source mechanism, probably on the same fracture.

Velocity model building and network design for improved event locations

In order to locate future microseismic events with higher accuracy and to additionally estimate source parameters, we have conducted a network design study. Based on a detailed 3-D model for both P- and S-wave velocities and density, we investigated propagation effects of microseismic wave fields using 3-D ray tracing, 3-D finite difference computations and first arrival times calculated by the Eikonal equation. Based on the observed waveform data and generally expected signal-to-noise ratios (SNR), we estimated a picking uncertainty for P- and S-wave onset times for a given microseismic event and network configuration. To improve future microseismic event locations and enable the estimation of source parameters, we suggest a network of at least 10 shallow boreholes (250 m) arranged in a spiral configuration to cover the main volume of interest and to obtain acceptable SNRs on a minimum of three

borehole arrays per event to allow for accurate locations (Figure 7). The computed location uncertainty is based on a bootstrap analysis, using the expected picking uncertainties. Events that occur within the network can be located with about ±250 m spatial and ±300 m depth resolution, assuming that events can be identified up to 4 km distance to the stations and that the events occurred at 1900 m depth (reservoir depth).

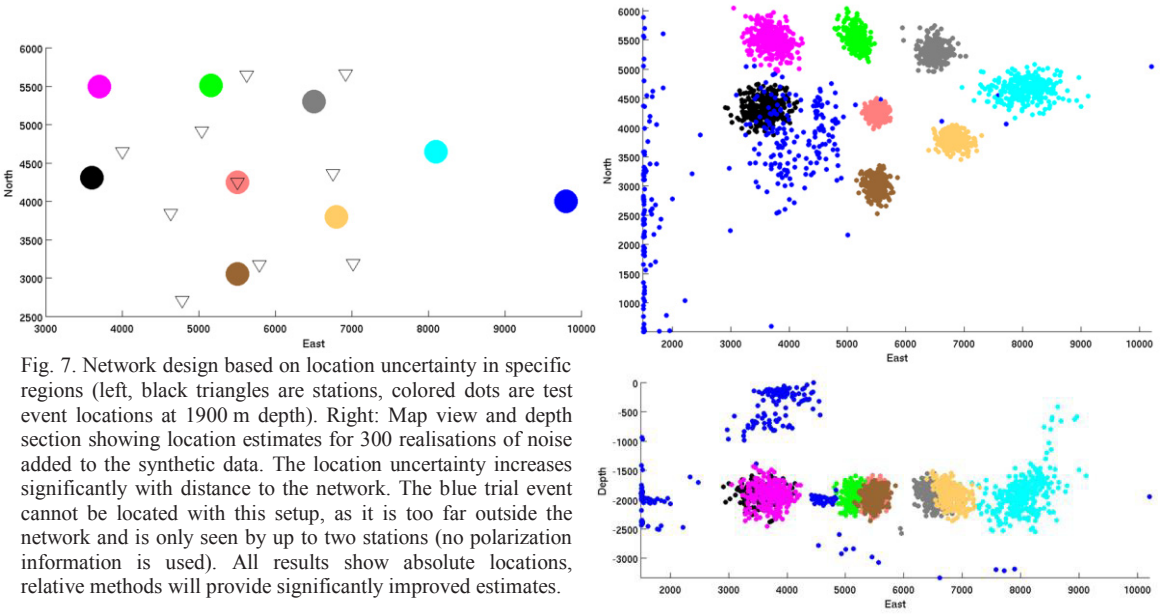

Fig. 7. Network design based on location uncertainty in specific regions (left, black triangles are stations, colored dots are test event locations at 1900 m depth). Right: Map view and depth section showing location estimates for 300 realisations of noise added to the synthetic data. The location uncertainty increases significantly with distance to the network. The blue trial event cannot be located with this setup, as it is too far outside the network and is only seen by up to two stations (no polarization information is used). All results show absolute locations, relative methods will provide significantly improved estimates.

Each borehole should consist of four three-component geophones to allow for data redundancy, differentiation between upward and downward propagating wave fields, and stacking of traces in case of weak signals. In case of larger events observed on the complete network, estimates of source mechanisms may also be provided. Inclusion of deeper borehole geophones, ideally close to reservoir depth would further enhance location accuracies, but this option was dismissed for economic reasons. However, the application of relative location methods, such as master-event or double-difference methods, permits the reduction of location uncertainty between events significantly.

Analysis of CO_2 injection data

Analysis of pressure versus injection rate data allows periods of matrix and fracture injection to be differentiated in the three CO_2 injection wells (KB501, 502, 503). The injection history can also be used to infer the reservoir fracture pressure and maximum matrix injection rate. The analysis shows that maximum applied pressure in all three wells has most probably exceeded the fracture pressure of the injection horizon for periods of time (Figure 8). The fracture pressure has been inferred from the relation between injection pressure and injection rate (Figure 9). Furthermore, we studied the injection history of the wells during 2010 to explore a possible relationship between microseismic and injectivity data (assuming that the microseismic events are related to fracturing in the injection horizon). The injection history at KB502 shows a period of fracture injection about mid-year, and at the same time, the number of microseismic events clearly increases. Wells KB501 and KB503, however, do not show clear evidence of fracturing during this time period. We therefore conclude that a sudden increase of microseismic activity implies formation fracturing, and thus provides a good monitoring technique to detect the exceedance of reservoir fracture pressure. In addition, the formation fracture pressure estimated with this method is above the previously estimated value. This also suggests that the cap rock fracture pressures may also be

higher than previously estimated. These findings are currently supported by other sets of data such as in-situ stress profile, empirically calculated fracturing pressure, Formation Integrity Test (FIT), and Leak Off Test (LOT).

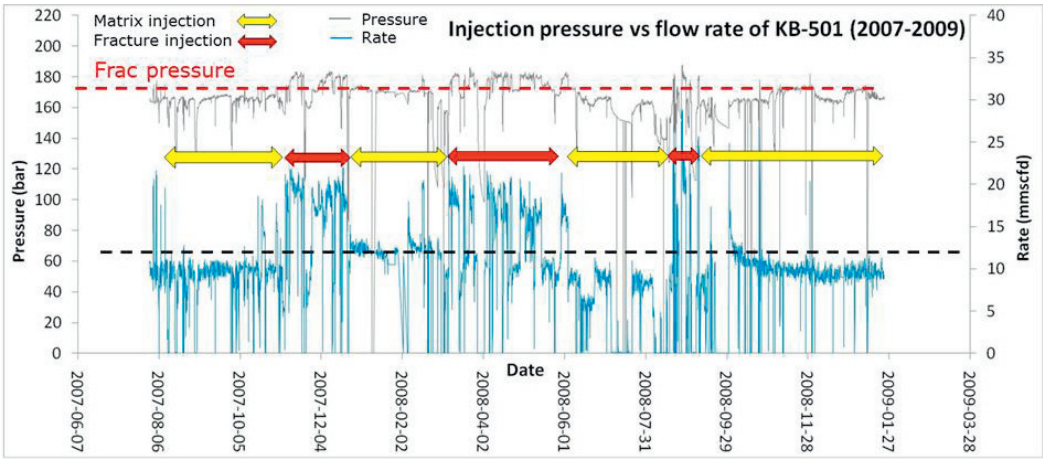

Fig. 8. When the injection pressure (dark blue) exceeds a certain level (reservoir fracture pressure, indicated by the red dotted line), the injection rate (light blue) increases strongly. Thus, we differentiate periods of matrix injection (yellow arrows) and fracture injection (red arrows).

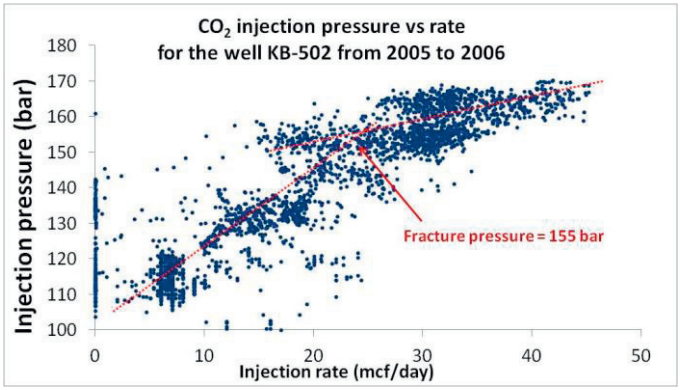

Fig. 9. Injection pressure versus injection rate; at about 155 bar, the two fitted lines intersect. At this pressure the injection rate increases suddenly with increasing injection pressure and this value of 155 bar is assumed to represent fracture pressure.

Conclusions

The analyzed microseismic data from the observation well (KB601) and the injection data at the Krechba CO_2 site shows a correlation between CO_2 injection periods and microseismic activity levels. Interpretation of well-head pressure data and injection rates identified periods of matrix and fracture injection, in agreement with the observation of increased microseismic event activity. The waveform cross-correlation results indicate that most events occur in clusters within a limited spatial area, and thus are likely to be related to Co2 injection. This demonstrates the potential value of microseismic monitoring for ensuring safe geological storage of CO_2. As best estimate for microseismic event locations detected with the downhole array, we computed S-P phase arrival times using a 3-D Eikonal solver and compared the computed travel times with the observed data. Together with directions from the polarization analysis, we obtain the most likely event locations as indicated in Figure 10. An extension of the monitoring system will significantly improve microseismic event locations, allowing us to locate and classify events with high accuracy.

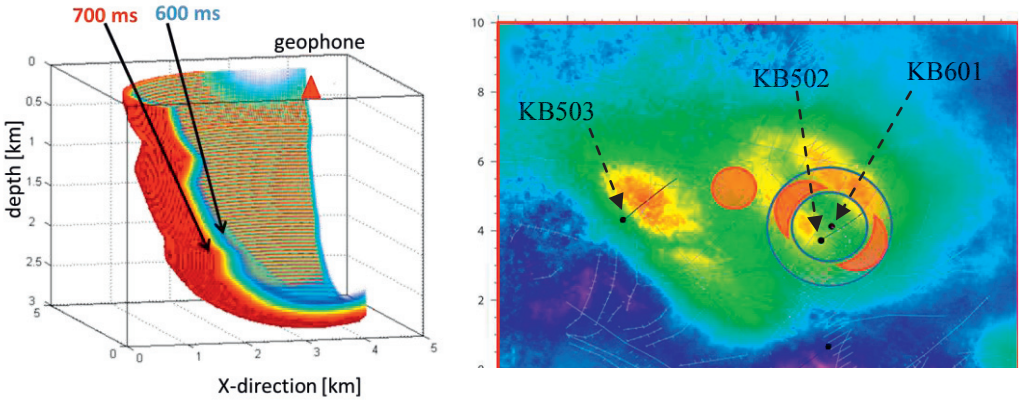

Fig. 10. Left: Theoretical S-P wave differential times as observed from one geophone. The color-coded bowl shows the potential locations of events with 600-700 ms S-P times. Adding the observation of polarization azimuths, we indicate the most likely locations on the map (right) with red shaded areas, assuming the events occurred close to or at reservoir depth. Grey lines are known faults. The background indicates the observed surface heave due to CO_2 injection.

Acknowledgements

NGI and NORSAR thank Gassnova (project no. 210267), the CLIMIT program of the Norwegian Research Council, and the In Salah JIP partners for financial contribution to the MIMOSA project. Berkeley Lab work was supported by the In Salah JIP and the Assistant Secretary for Fossil Energy, through the National Energy Technology Laboratory, under the U.S. Department of Energy Contract No. DE-AC02-05CH11231. The authors like to acknowledge In Salah Gas Joint Venture and their partners BP, Statoil, and Sonatrach for providing field data and valuable discussions. We also thank K. Iranpour, P. Zhao and K. Tronstad for their contribution to this work.

References

[1] O. Eiken, P. Ringrose, C. Hermanrud, B. Nazarian, T.A. Torp, L. Høier, Lessons learned from 14 years of CCS operations: Sleipner, In Salah and Snøhvit, Energy Procedia, 4 (2011) 5541-5548.

[2] D.W. Vasco, A. Rucci, A. Ferretti, F. Novali, R.C. Bissell, P.S. Ringrose, A.S. Mathieson, I.W. Wright, Satellite-based measurements of surface deformation reveal fluid flow associated with the geological storage of carbon dioxide, Geophys. Res. Lett., 37 (2010) L03303.

[3] R.C. Bissell, D.W. Vasco, M. Atbi, M. Hamdani, M. Okwelegbe, M.H. Goldwater, A full field simulation of the in Salah gas production and CO2 storage project using a coupled geo-mechanical and thermal fluid flow simulator, Energy Procedia, 4 (2011) 3290-3297.

[4] J. Rutqvist, H.-H. Liu, D.W. Vasco, L. Pan, K. Kappler, E. Majer, Coupled non-isothermal, multiphase fluid flow, and geomechanical modeling of ground surface deformations and potential for induced micro-seismicity at the In Salah CO2 storage operation, Energy Procedia, 4 (2011) 3542-3549.

[5] L. Gemmer, O. Hansen, M. Iding, S. Leary, P. Ringrose, Geomechanical response to CO2 injection at Krechba, In Salah, Algeria, First Break, 30 (2012) 6.

[6] A. Mathieson, J. Midgley, K. Dodds, I. Wright, P. Ringrose, N. Saoul, CO_2 sequestration monitoring and verification technologies applied at Krechba, Algeria, The Leading Edge, 29 (2010) 216-222.

[7] V. Oye, M. Roth, Automated seismic event location for hydrocarbon reservoirs, Computers & Geosciences, 29 (2003) 851-863.